**ORIGINAL PAPER**

# The Failure and River Blocking Mechanism of Large-Scale Anti-dip Rock Landslide Induced by Earthquake

**Wen-Jie Xu[1] · Lin Wang[2] · Kai Cheng[3]**

## Abstract

Landslide and river blocking induced by earthquakes have occurred widely in nature. The topography and geological structure of slopes have a considerable influence on the geotechnical structure of the formed landslide dam. In the Hongshiyan valley (Niulan river, Yunnan province, China), a large-scale anti-dip rock landslide was triggered by Ludian earthquake in 2014 with more than $1.36 \times 10^7$ m$^3$ of displaced rock, which formed a barrier lake with an estimated volume of $2.6 \times 10^8$ m$^3$. In relation to this example, the whole process from triggering, failure, disintegration, to landslide dam formation blocking a river is simulated using the discrete element method (DEM). For this, a 3D DEM modeling methodology of the complex landslide is proposed that includes an inversion strategy which uses laboratory tests of rock samples from the landslide to obtain the numerical parameters for the DEM. Initial investigations indicate that the weak slope base is an important internal factor resulting in the failure of the slope. During the earthquake, this part of the slope is the first to disintegrate and flow out under the upper rock mass pressure. This exposes the upper rock mass to large domains of tensile stress that eventually leads to the failure and disintegration of the upper hard rock mass. The anti-dip bedding of the slope results in a landslide dam consisting of "fine particles at the lower elevations and coarse rock blocks deposit at the higher elevations". Our model also suggests that the triggering and failure mode of the landslide may mostly depend on the external factors (such as earthquake, rainfall, and river erosion and so on), while the subsequent dynamic process of the landslide and the engineering geological structure of the landslide dam mainly depend on the geological structure of the slope, sliding distance and topography of the valley.

## Highlights

- A typical "weak base" anti-dip layered rock landslide induced by earthquake has been introduced.
- A method for the 3D DEM complex model generation of landslide is proposed.
- The whole process of the landslide and river blocking process have been studied by using DEM.
- The geological structure of the barrier dam is controlled by the slide body, runout distance and topography of valley.

✉ Wen-Jie Xu
wenjiexu@tsinghua.edu.cn

1   State Key Laboratory of Hydroscience and Hydraulic Engineering, Department of Hydraulic Engineering, Tsinghua University, Beijing 100084, People's Republic of China

2   State Key Laboratory of Eco-Hydraulics in Northwest Arid Region (Xi'an University of Technology), Xi'an 710048, People's Republic of China

3   China Power Kunming Engineering Corporation Limited, Kunming 650051, Yunnan, People's Republic of China

## 1 Introduction

A large number of investigations have indicated that an earthquake is a major contributor in the triggering of landslides. An intense earthquake may lead to thousands or tens of thousands of landslides within an area as large as 100,000 km$^2$ (Keefer 2002). For example, the 1994 Northridge earthquake ($M_s$ 6.5) in the USAd States triggered about 11,000 landslides over an area of about 10,000 km$^2$ (Harp and Jibson 1996); the 2008 Wenchuan earthquake ($M_s$ 8.0) triggered
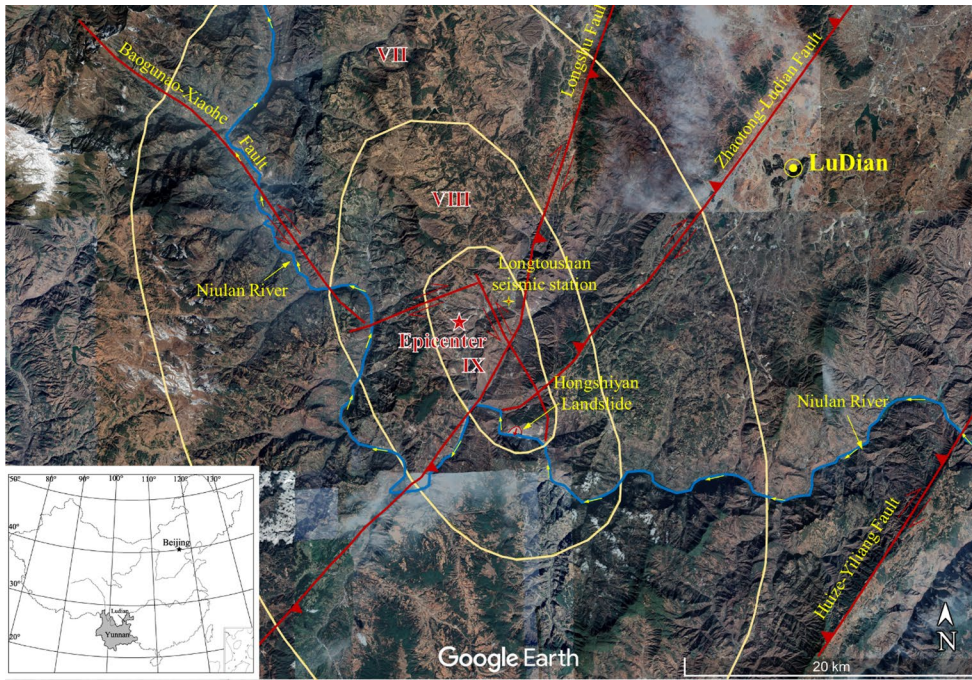
**(a)**
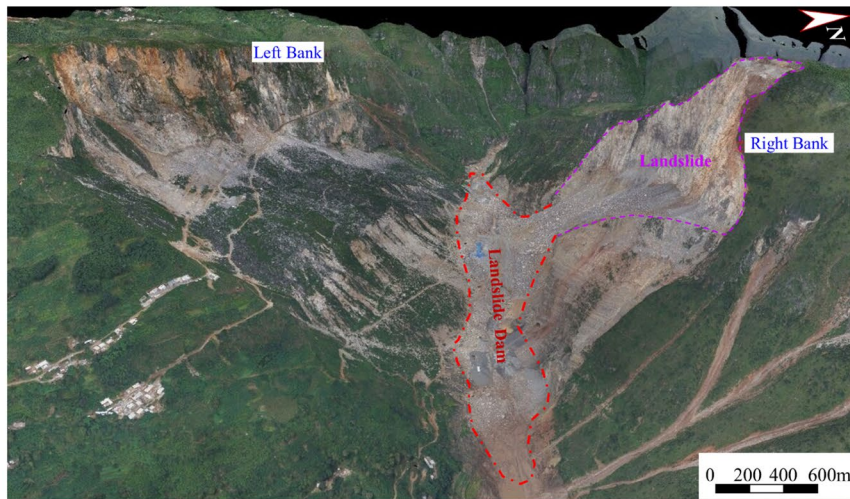


**(b)**
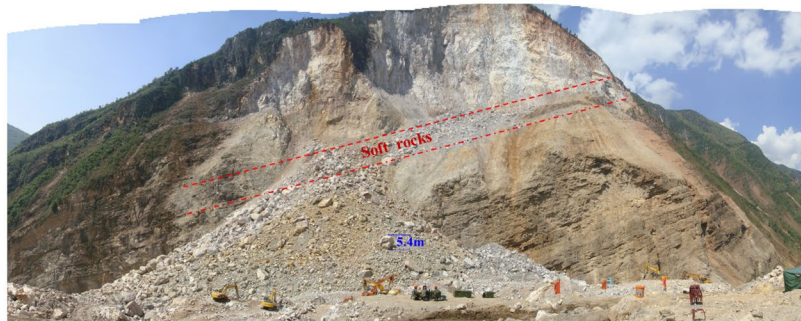


**(c)**

about 200,000 landslides and more than 87,000 casualties were reported (Fan et al. 2018); and about 6000 landslides resulted from the Hokkaido Iburi-Tobu Earthquake on September 6, 2018 (Yamagishi and Yamazaki 2018).

China is a mountainous country, with mountainous terrain accounting for two-thirds of its total surface area. Furthermore, China lies between the two most active seismic belts in the world, namely the Pacific seismic belt in the east and the Himalaya–Mediterranean seismic belt in the south. Intense earthquakes are widespread in China, especially in the south-west (Fan et al. 2018). Landslides that are induced by an earthquake are widely distributed, and mostly runout at high speeds. As a result, these landslides cannot be ignored and are attracting worldwide attention among scholars: in particular, the study on earthquake-prone areas (especially those in mountainous areas) and the resulting secondary geological hazards. These include landslide dams that induce the secondary hazard of flooding because of river blockages, especially in gorges. For example, about 828 landslide dams were formed during the 2008 Wenchuan earthquake (Fan et al. 2018). Landslides which occurred in gorges are characterized as high speed and short runout in which the slide body is confined in the gorge and eventually forms a landslide dam (Xu et al. 2013). As the running distance is very short, the mechanism and the structure of the deposit (or landslide dam) are greatly different from that of the long-runout landslide.

Numerical methods are now widely used in geotechnical engineering to analyze the stability and failure process of the slope, tunnel, etc. Among these, applying explicit dynamic FEM, Xu et al. (2013) studied the 3D slope failure process and landslide generation under earthquakes. Especially, for the advantages on the simulation of the failure process of geomaterials, discrete element method (DEM) on 2D (Tang et al. 2009; Bozzano et al. 2011; Song et al. 2016) and 3D (Lo et al. 2011; Lin and Lin 2015; Wu et al. 2018; Zhou et al. 2019; Wang et al. 2020), discontinuous deformation analysis method (Wu 2010; Wu et al. 2017; Zhang et al. 2013), and combined finite-discrete element method (Barla et al. 2012; Feng et al. 2017) have been widely used for the modeling of the slope failure processes. Using 3D smoothed particle hydrodynamics (SPH), Dai et al. (2011) studied the landslide failure process induced by the 2008 Wenchuan earthquake, but the seismic wave and rock structures were not considered. Although a number of studies have been done on the simulation of the landslide mechanisms under seismic activity, the majority of them are based on 2D models or have

oversimplified the geological structure of the landslide. With the advancement of the numerical techniques and computing resources, sophisticated models can now be developed that study the failure processes of landslides under seismic activity.

River blocking is common for landslides in gorges, and the geological structure of landslide dams is important for evaluating the secondary hazards induced by the dam breach. The Hongshiyan landslide which was triggered by the 2014 Ludian earthquake ($M_s$ 6.5), Yunan, China, serves as a reminder of the consequences. This study uses 3D DEM to model the failure processes of the Hongshiyan landslide and analyze the mechanism and the structure characteristics of the landslide dam from the numerical results. The results are validated on the data obtained from a field investigation after the incident. The outcomes of this study will be useful for the theoretical research and the reduction of landslides hazards in gorges.

## 2 Geologic Overview of the Landslide

On August 3, 2014, a $M_s$ 6.5 earthquake occurred in Ludian county, Yunnan, China, which triggered a large-scale landslide (Fig. 1) in the Hongshiyan village on the Niulan River and formed a barrier lake with an estimated capacity of $2.6 \times 10^8$ m³ due to the river blocking. The epicenter of the earthquake is located at 27.11° N, 103.35° E, with a shallow focal depth of 12 km, and triggered by the nearly vertical sinistral strike-slip Baogunao–Xiaohe fault which trends approximately N40W° (Fig. 1a; Xu et al. 2015; Chang et al. 2016).

The Hongshiyan landslide, located about 8.8 km southeast of the epicenter (Fig. 1a), along the river was about 890 m long with a height of about 500 m and total volume of about $1.36 \times 10^7$ m³. The slopes on both sides of the Niulan River in the landslide area are steep, with the slope angle of about 70°–85° and the height of about 700 m. Based on the field investigation, the rock stratum in the landslide generally dips downstream and toward the right bank, with the strata strike and dip of about 290°–330° ∠ 10°–30° (Fig. 2a). No large-scale faults were found in the landslide area, but tension joints that developed in the rock stratum were divided into two groups (Fig. 2a): $J_1$ (190°∠80–83°), which is approximately parallel to the river valley, formed by an unloading effect and extends in length; $J_2$ (60°∠80°), which is approximately perpendicular to the valley and formed by dissolution.

The rock strata in the landslide area can be divided into three parts from top to bottom (Fig. 2b):

1. The upper part consists of Permian ($P_1^m$) thick bedded limestone dolomite and Permian ($P_1^q$) dolomite lime-

**Fig. 2** Geological map of the Hongshiyan slope: **a** engineering geological map; **b** geological profile of the failed slope



(a)



(b)
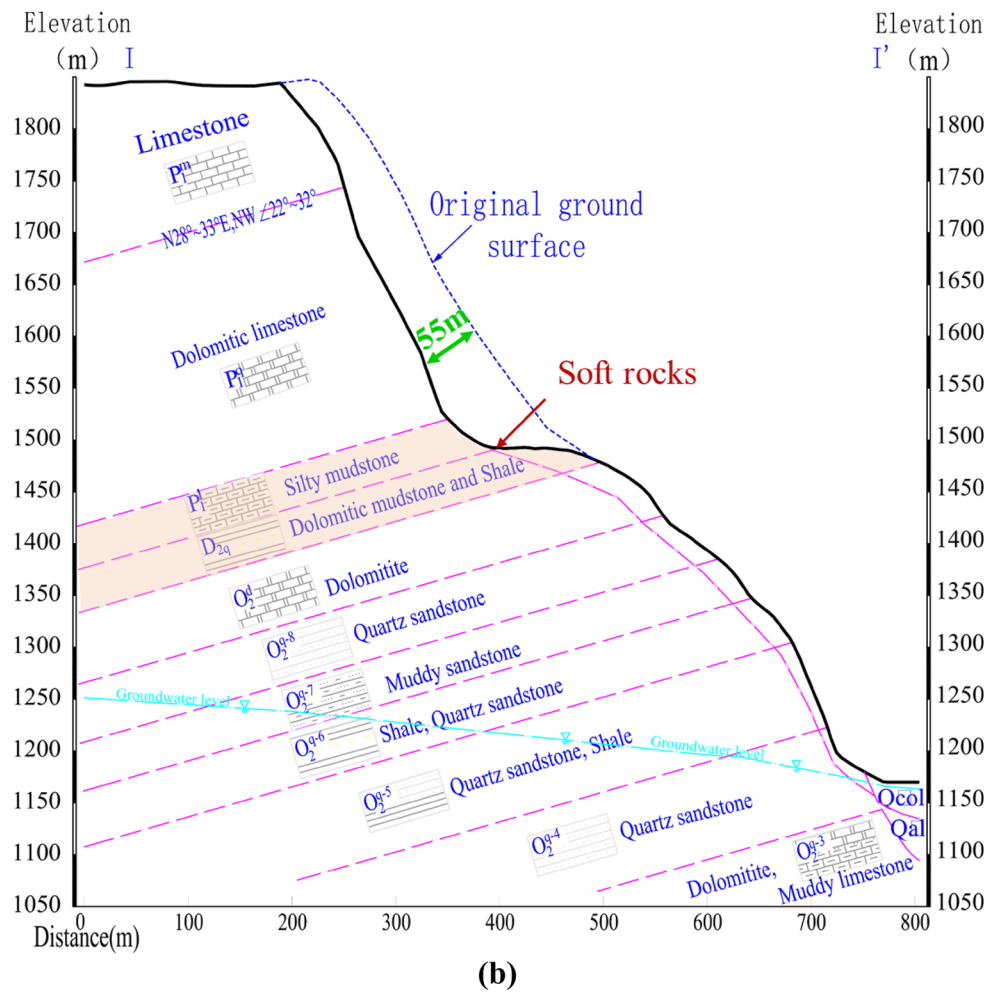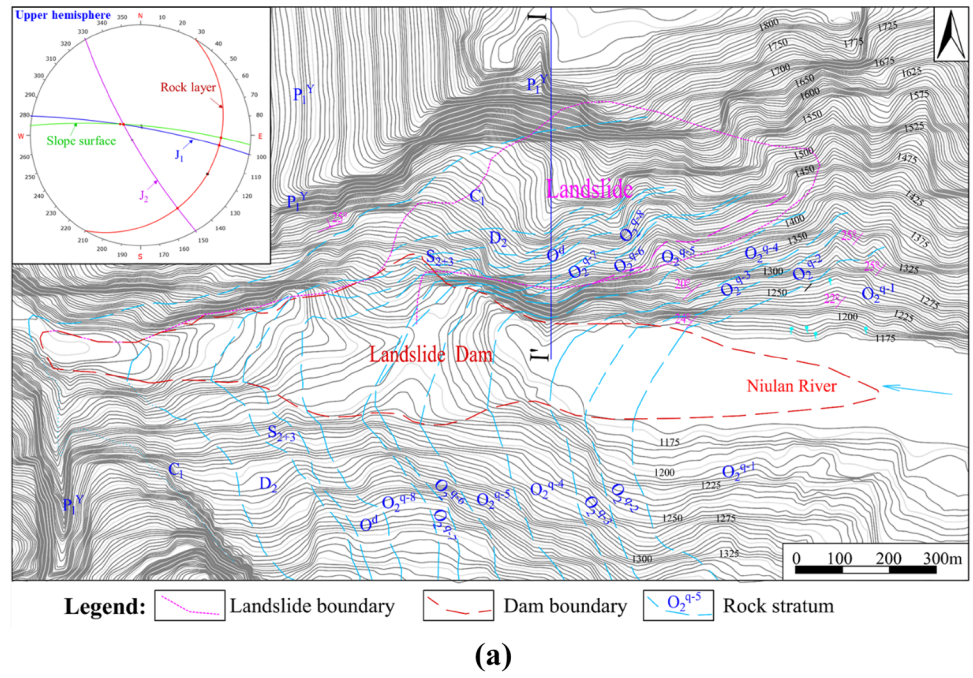
stone, with high strength rock. Cutting by J1 and J2, the rock masses of the part are classed as "very blocky" to "blocky" structure (Luo et al. 2019).

2. The middle part is composed of the Permian ($P_1^1$) silty mudstone and Devonian ($D_{2q}$) dolomitic mudstone and shale, with strongly weathered and lower strength rock. The rock masses are classed as "disintegrated" to "distributed" structure (Luo et al. 2019).

3. The lower part is composed of the Ordovician ($O_2$) medium- to thin-bedded quartz sandstone, shale and dolomite, forming an interlayer structure with soft and hard rock strata.

Therefore, the geological structure of the slope is that of a weak base and anti-dip rock slope with the hard rock strata at the upper parts and relatively weak rock strata at the middle and lower parts (Fig. 2b). The formation of the river valley is due to erosion by the ancient Niulan River. During erosion, the slopes on both sides become steeper where unloading deformation occurred; on the other hand, under the long-term effect of gravity, the weak rock was slowly deforming, which resulted in gradual deformation and fracturing of the upper hard rock. Eventually, a series of fractures ($J_1$) parallel to the river valley were formed in the upper hard rock strata.

During the earthquake, the rock strata at the upper part of the slope become unstable and collapse along the soft rock in the middle and then accumulate in the valley to form a landslide dam that eventually blocks the Niulan River stream. Based on the topography (Fig. 1), the Hongshiyan landslide dam's right bank is high and its left bank is low, where a number of large rock blocks have accumulated at the right edge of the bank (Fig. 1c). The elevation of the lowest point at the dam crossing the river is 1222 m, and that of the highest point on the left bank is 1240 m. The slope ratio of the upstream face is about 1:6, and that of the downstream face is about 1:10–1:4. The bottom of the dam along the river is about 910 m wide and the axial length of the dam at the elevation of 1222 m is about 307 m.

According to the field investigation and boreholes datum, the major part of the landslide dam is composed of large rock blocks, and there is an obvious difference in the geological properties between the upper and the lower parts of the dam, which are constituted as the following:

1. Elevation above 1180 m: this part is mainly composed of large rock blocks that contain only few fine particles that are loosely accumulated. Based on the field permeability tests, the permeability coefficient of this part is about $5.0 \times 10^{-2}$ cm/s; the rock blocks mainly consist of weakly weathered or fresh dolomitic limestone and dolomites, in which the maximum size of the rock blocks exceed 5 m (Fig. 1c). According to the field investigation, measurement based on 3D scanner and

sieving analysis, the rock blocks with a particle size exceed 50 cm accounting for about 30% of the mass, those with the size 2–50 cm account for about 45% of the mass, and those with size less than 2 cm account for only about 25% of the mass.

2. Elevation below 1180 m: this part is mainly composed of a mixture of larger rock blocks, finer gravels and sands. Some locations are covered with sand inter-bedded with rock blocks and gravel, with a continuous particle size distribution, high density, low porosity and permeability coefficient of about $5.0 \times 10^{-3}$ cm/s.

Therefore, the engineering geological structure of the Hongshiyan landslide dam generally presents the characteristics of "fine particles at the lower elevations and coarse rock blocks at the higher elevations", which is different from that (Xu et al. 2013) of the Tangjiashan landslide (bedding landslide) induced by the Wenchuan earthquake in 2008, featuring "fine particles at the higher elevations, coarse rock blocks at the lower elevations".

# 3 Numerical Method for Kinematics of the Landslide

## 3.1 Discrete Element Method (DEM)

DEM, firstly proposed by Cundall and Strack (1979), plays an increasingly important role in geotechnical engineering. In DEM, the simulated domain is divided into a series of rigid particles and can be used to simulate the failure processes of granular materials, geotechnical materials and landslides. In every time step, all particles need to resolve contact, estimate interaction forces and moments based on constitutive laws and then update their location based on Newton's second law. In this study, an extendable open-source framework based on the DEM, named as YADE (Kozicki and Donze 2009), is used to perform the numerical simulation.

To better simulate the failure process of the rock, an enhanced contact model (Fig. 3) was programmed into YADE (Scholtes and Donze 2012, 2015), which can not only simulate intact layered rock, but also pre-existing discontinuities (such as joints and bedding planes) following the smooth-joint contact approach of Ivars et al. (2008). Details of the numerical implementation are available in Scholtes and Donze (2012, 2015) and are not repeated here.

In DEM, if the contact forces between the two particles satisfy the fracture criterion as shown in Fig. 3, the cohesion strength between the particles becomes zero and only friction exists (Scholtes and Donze 2012, 2015). The contact fracture area between two particles A and B is given by:
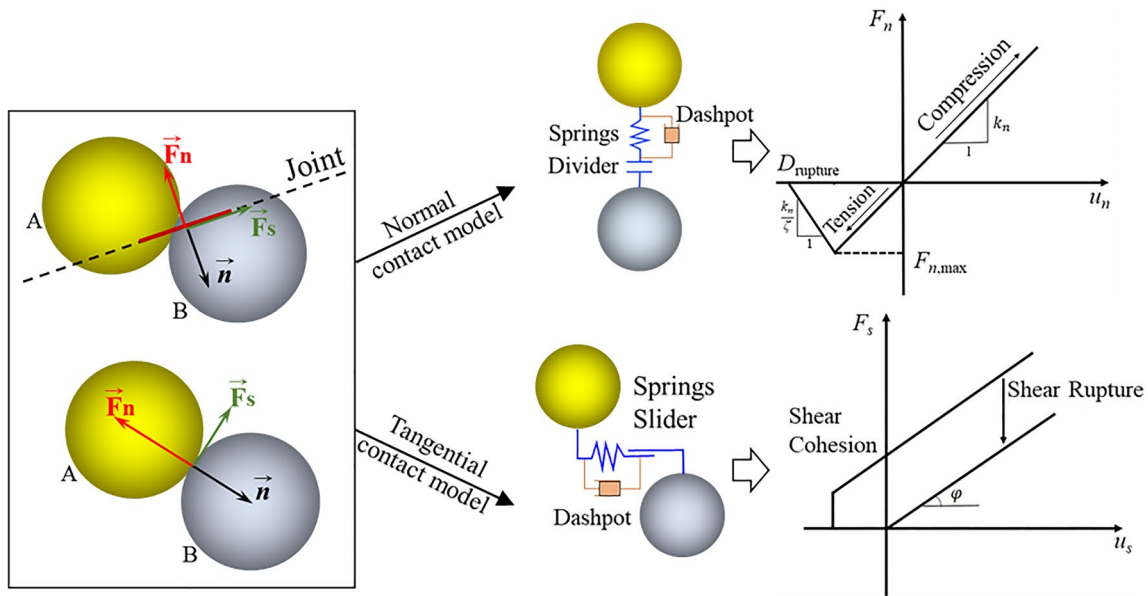
**Fig. 3** Contact model between two adjacent particles

$$FA = \pi \cdot \left( \frac{R_A + R_B}{2} \right)^2, \tag{1}$$

where $R_A$ and $R_B$ are the radii of particle $A$ and particle $B$, respectively, with bonded fractures. To quantitate the description of the fracture development degree under the external loads, the fracture ratio (FR) is computed as follows:

$$FR_t = \sum FA_t / V, \tag{2}$$

where $FR_t$ is the fracture ratio at moment $t$, $\sum FA_t$ is the total area of all fractures at moment $t$, and $V$ is the volume of the simulated domain.

Furthermore, a damping ratio of 0.02 is used in the DEM simulation of this study.



**Fig. 4** DEM model generation process of the landslide body
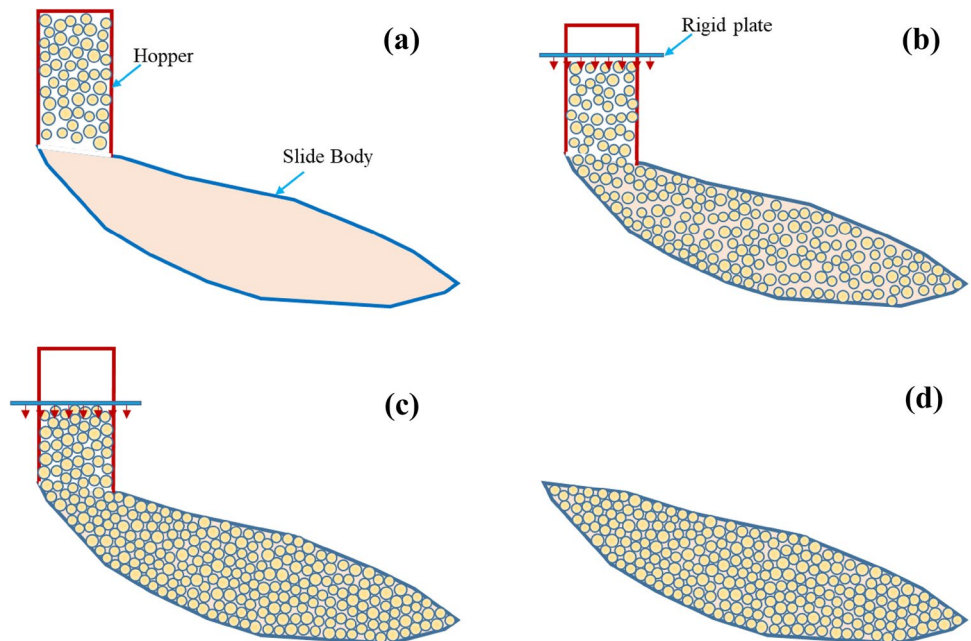
## 3.2 3D Geological Structure of the Slope

When using DEM for a landslide simulation, it is necessary to characterize the slope model by using an aggregation of particles that are tightly in contact. This is due to the fact that the composition and compactness of particle aggregates will greatly influence the numerical results. Generally, the slope topology in nature is complex, so it is difficult to generate the full details in a 3D DEM model. In this study, a method to generate a 3D DEM model of the slope is presented (Fig. 4):

1. The 3D geometric model of the slope is constructed according to the field measurement datum, and a rectangular hopper with a volume of about 1/5 to 1/3 times of the slide body's volume is generated at the top of the slope (Fig. 4a). In the hopper, a series of spherical particles are randomly generated according to the given particle size distribution.
2. Based on DEM, the slide body and the hopper can be set as the boundary of the simulation, where the spherical particles in the hopper fall into the slide body under gravity. This step needs to be repeated until the slide body is filled with spherical particles. To generate a relatively dense aggregate of particles, smooth particles are used in DEM.
3. Once the slide body is full of particles, a pre-compression load (1 MPa in this study) is applied on the rigid plate above the hopper to compact the aggregate constituting the slide body into a dense packing as outlined in Fig. 4b.
4. After the load on the rigid plate was stabilized (Fig. 4c), the particles outside the landslide body were removed, and the DEM model of the landslide body is generated (Fig. 4d).

According to the geological structure of the Hongshiyan slope, the 3D geometric model of the slide body is constructed and used to generate the corresponding 3D DEM model. The radii of spherical particles that are used in this study are uniformly distributed from 1.0 to 1.2 m, and a total number of 295,985 particles are required for the slope generation of the DEM model (Fig. 5a). The void ratio of the particles' aggregate is 0.56. Figure 5b shows the 3D DEM model of the Hongshiyan slope. The slide bed and the slope terrain are represented by a series of triangular meshes. To better simulate the landslide process, according to the geological structure of the Hongshiyan slope, it can be divided into two parts: the upper part (blue part in Fig. 5b) is dolomite and dolomitic limestone with higher strength; the lower part (yellow part in Fig. 5b) is a shale formation with relatively lower strength. According to the occurrence of the rock stratum measured in the field, the average value of strike and dip, 310°∠20°, is used to model the structure of the rock mass composing the slope, with the thickness of the stratum being around 5 m.

## 3.3 Inversion of Rock Parameters

It is very difficult to obtain the contact parameters of the particles used in DEM directly by experiment. The values of these parameters are the most important factors to control the whole landslide process including the triggering, failure and movement of the slope. To obtain reasonable meso-mechanical parameters of DEM particles in the slide body constituting the major rock (dolomite), a series of laboratory tests are carried out and the results are then used for the DEM parameter inversion. The steps are as follows:

1. Stress–strain behaviors of the typical rock. Using the rock samples of the slope (5 cm in diameter, 10 cm in height), uniaxial and triaxial tests (confining pressure: 3 MPa and 6 MPa) are conducted to obtain the macroscopic stress–strain behaviors of the rock and the results will be used for the meso-mechanical parameters inversion of the corresponding DEM particles.
2. DEM model for inversion tests. A cylindrical sample with the same particle size distribution (1–1.2 m in radius) and the same void ratio (0.56) as that of the landslide is modeled in DEM for numerical testing. To reduce the sensitivity of the particle size on the results, a rock sample of 40 m in diameter and 80 m in height is modeled. Following these choices, the total number of particles in the rock sample is 11,025 (Fig. 6a). Since there are no visible joints in rock samples used in laboratory tests, the joints are not considered in the numerical model.
3. DEM numerical tests. Based on the DEM numerical sample model, numerical tests with the same conditions as the laboratory tests were conducted (Fig. 6). In DEM tests, to set the flexible confining pressure boundary, a series of independent rigid plates (Fig. 6b) are used to produce the lateral confining pressure equivalent to that of which is applied in laboratory tests by the servo control. Following this, an axial strain is applied by two rigid plates located at the top and bottom of the sample at a velocity of 0.01 mm/s in opposite directions. The joint rock model (Scholtes and Donze 2012, 2015) shown in Fig. 3 is used for contact between the particles characterizing the rock sample. Smooth contact is used to model contact between the lateral plates and the particles; and frictional contact is used to model contact between the loading plates and the particles.
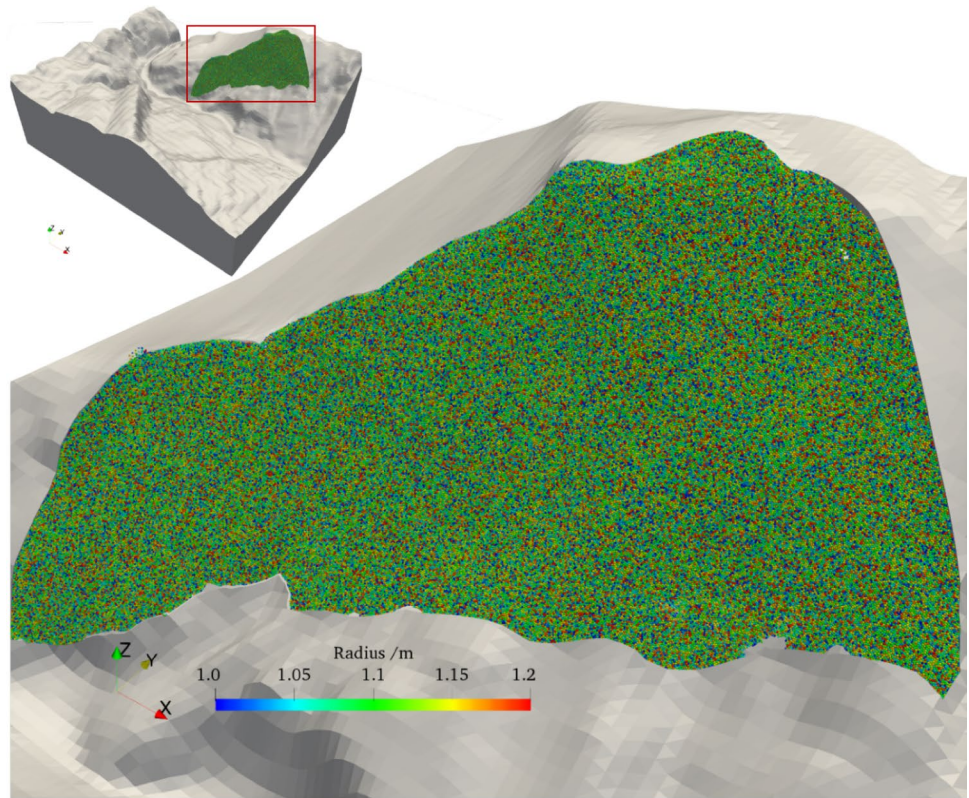
**(a)**
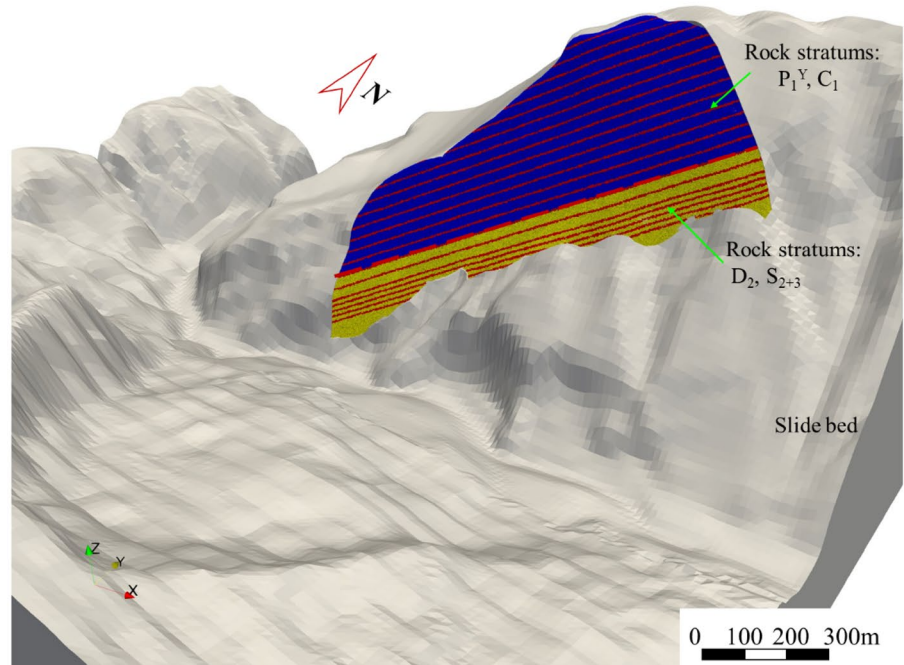


**(b)**

**Fig. 6** DEM triaxial test of the rock sample: **a** DEM model of the rock sample; **b** flexible boundary for confining stress
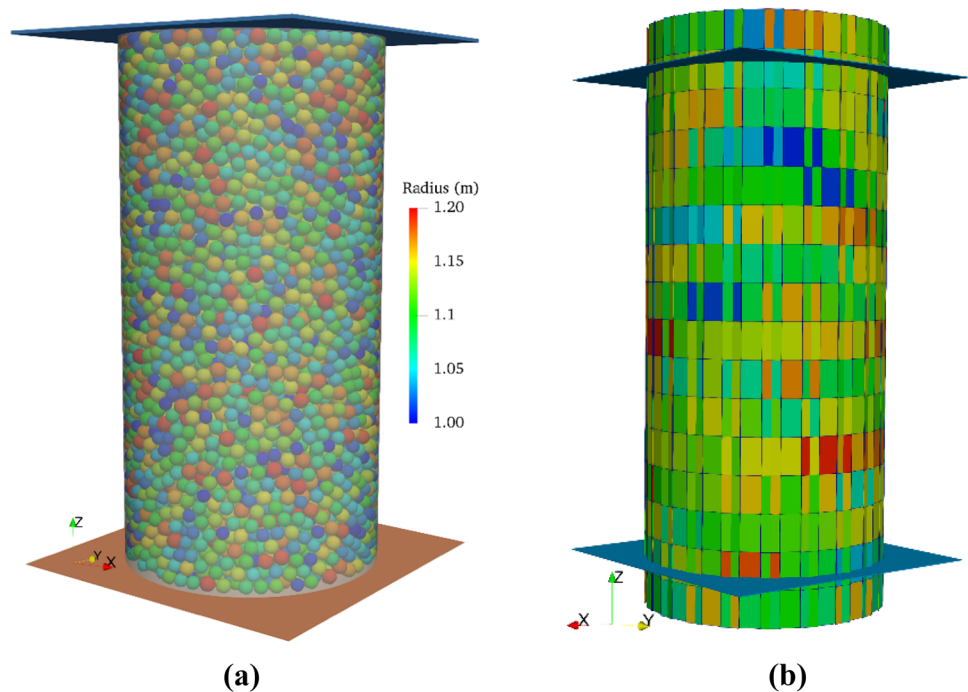


(a)

(b)

**Table 1** The parameters of DEM particles for dolomite

| Parameters | Values |
|---|---|
| Particle density (kg/m³) | 3900 |
| Young's modulus (GPa) | 22 |
| Poisson's ratio | 0.5 |
| Tensile strength (MPa) | 6.5 |
| Cohesive strength (MPa) | 65 |
| Friction angle (°) | 20 |
| Residual friction angle (°) | 15 |

4. DEM inversion parameters setting. The meso-mechanical parameters and contact parameters that are identified during inversion include: Young's modulus ($E$), Poisson's ratio ($v$), tensile strength ($T$), cohesive strength ($c$), friction angle ($\varphi$) and so on, among which $T$, $c$ and $\varphi$ mainly control the strength of the sample and behavior after failure. The normal contact stiffness ($K_n^{AB}$) and tangential contact stiffness ($K_t^{AB}$) between two contacting particles ($A$ and $B$) are calculated from (Smilauer et al. 2015):

$$K_n^{AB} = \frac{E^A R^A E^B R^B}{E^A R^A + E^B R^B}, \tag{3}$$

$$K_t^{AB} = K_n^{AB} \cdot \frac{v^A + v^B}{2}, \tag{4}$$

where the superscripts $A$ and $B$ are the particles identifiers, and $R$ is the radius of the particle. Both $E$ and $v$ control the

elastic behaviors of the sample, and in this study the particles' $v$ is set as 0.1.

In the uniaxial test, the stress–strain behavior of the sample is mainly affected by $E$, $T$ and $c$. Therefore, $E$, $T$ and $c$ are taken as the inversion parameters to prepare the orthogonal tests, and $\varphi$ is take as a fixed value of 30°. Then a series of uniaxial numerical tests are conducted and compared with that of the laboratory tests. A group of $E$, $T$ and $c$ with the stress–strain behaviors mostly corresponding with that of the laboratory test are taken as the final inversed parameters. Based on the obtained $E$, $T$ and $c$, the triaxial numerical tests with confining pressure of 3 MPa are performed to inverse $\varphi$. Similarly, the $\varphi$ value with the macroscopic stress–strain curve of the numerical result, which mostly corresponds to that of the laboratory test, is used as the final value of the friction angle. Table 1 shows the inverse parameters for DEM simulation of the dolomite composing the slope.

Figure 7 shows the stress–strain curves from numerical tests and the sample fracture characteristics with the parameters are presented in Table 1. The confining pressures of 0 MPa and 3 MPa are used as references to obtain the inverse DEM parameters; and the confining pressure of 6 MPa is used to test the obtained parameters (Table 1) to verify whether these parameters can reasonably reflect the deformation and mechanical behavior under other confining pressures. Through the comparison of the numerical and laboratory test results (Fig. 7), it can be seen that not only the results for the reference cases (0 MPa and 3 MPa), but also the test results of 6 MPa confining pressure agree with the experiments results well.
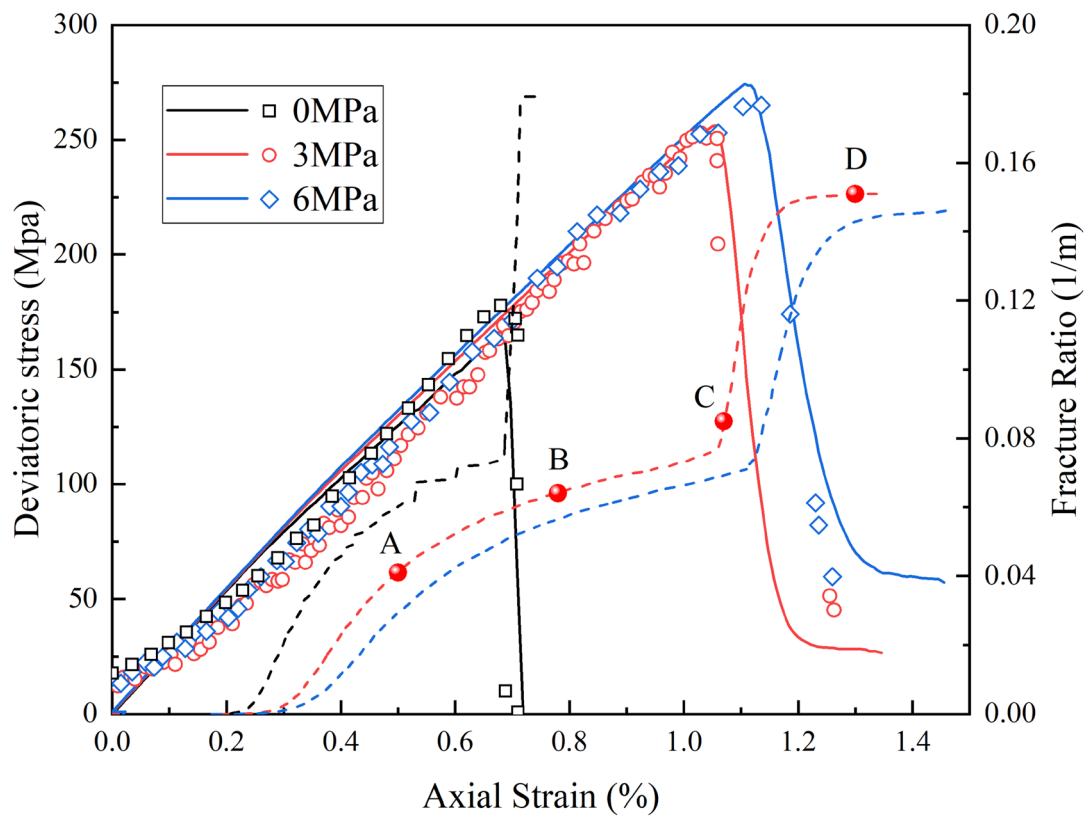
**(a)**
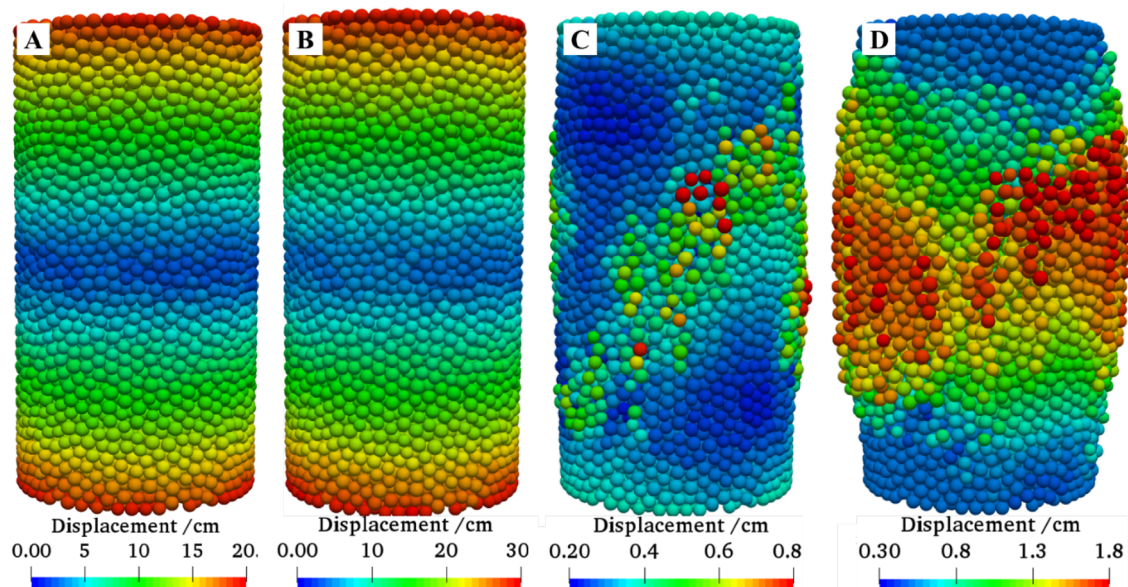


**(b)**

**Fig. 7** Stress–strain relationships and the fracture process of the rock sample: **a** evolution of the stress and fracture ratio with axial strain (the void symbols are results of the laboratory tests; the solid lines are results of the numerical test; the dotted lines are the fracture ratio of the sample from the numerical test); **b** deformation characteristics of the sample at different stages (the deformation of the sample is magnified twice)

Based on the fracture characteristics of the sample (Fig. 7), prior to reaching the peak intensity, the fracture ratio (FR) rises slowly, and the sample's internal fractures (cracks) are in the aggregation and development stage. Meanwhile, as the axial strain increases, the fractures localize gradually. When the stress reaches the peak strength, FR increases rapidly, and the fractures are connected inside the sample, forming multiple connected fracture faces. Finally, the stress decreases sharply, while the fracture faces develop gradually and the rock sample breaks eventually. From the above analysis, it can be seen that the macroscopic stress–strain behavior and fracture processes of the rock sample obtained by the numerical simulation are consistent with the laboratory results. Therefore, the parameters in Table 1 can reflect the strength and deformation behavior of the rock composing the slope, which provides a basis for the subsequent simulation of the slope failure processes.

**Table 2** Contact parameters of particles for the shale and rock joints

| Material | Parameters | Values |
|---|---|---|
| Shale | Particle density (kg/m³) | 3900 |
| | Young's modulus (GPa) | 20 |
| | Poisson's ratio | 0.5 |
| | Tensile strength (MPa) | 1.3 |
| | Cohesive strength (MPa) | 13 |
| | Friction angle (°) | 20 |
| | Residual friction angle (°) | 15 |
| Rock joints | Normal stiffness (GPa m) | 30 |
| | Shear stiffness (GPa m) | 15 |
| | Tensile strength (MPa) | 0 |
| | Cohesive strength (MPa) | 0 |
| | Friction angle (°) | 20 |
| | Dilation angle (°) | 10 |

Additionally, the laboratory tests show that the natural density of dolomite constituting the slope is about 2.5 g/cm³. The density of DEM particles is obtained from inversion as 3.9 g/cm³ based on the comparison of the mass between the DEM sample (with void ratio 0.56) and real rock sample with the same volume.

To characterize the strength of soft rock (shale) at the lower part of the slope, its cohesive and tensile strength are set to 1/5th of upper hard rock (dolomite), while the cohesive and tensile strengths' value of the joints (rock planes) are not considered (their values are set as zeros). Table 2 presents the mesoscopic contact parameters of shale and joints which are used for the simulation. Furthermore, using the parameters shown in Tables 1 and 2, the slope is in a stable state under gravity.

### 3.4 Load and Boundary Conditions

Since the landslide occurred in the shallow strata, the tectonic stress is not considered, and only the gravity and seismic loads are applied. The gravity is set as 9.81 N/kg, and a global damping of 0.02 is used during the numerical simulation. The time step of the numerical simulation is $5 \times 10^{-4}$ s. The simulation of the slope dynamics is divided into two steps:

1. Gravity. The landslide bed is fixed and gravity is applied, until the unbalanced force in the system is less than 0.001 N, which ensures the slope achieves equilibrium under gravity.
2. Seismic wave. As the gravity loading step is finished, the seismic waves in the directions of $E-W(x)$, $-S(y)$ and $-D(z)$ are applied at 0.05 s intervals. In DEM, the

**Fig. 8** Velocity diagram based on the 2014 Ludian earthquake record from the seismic station at Longtoushan (Fig. 1a), after a baseline correction
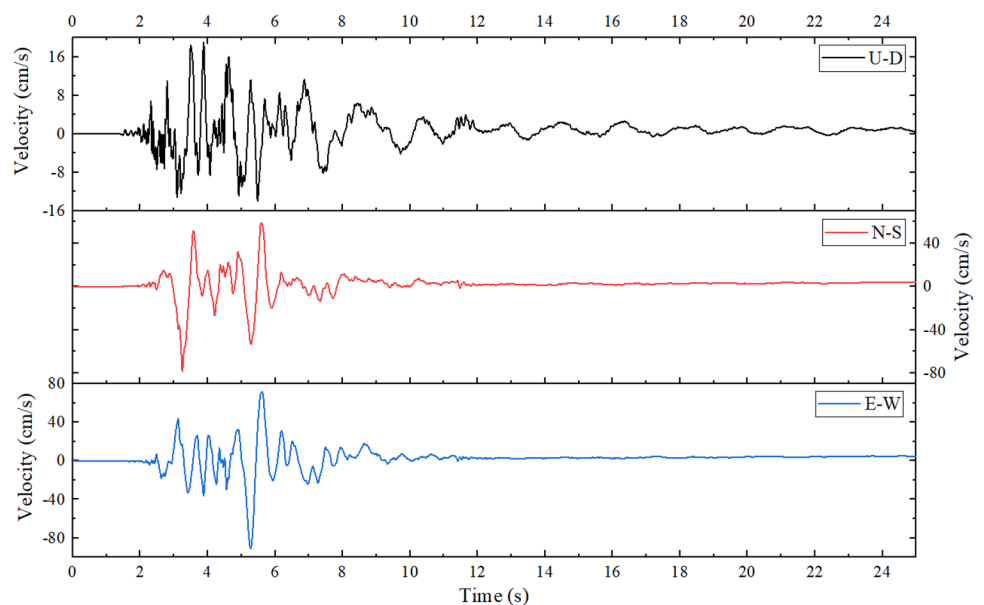
acceleration boundary is applied generally by applying the velocity on the boundary (slide bed in this study, Fig. 5). Therefore, in this study the velocity is applied to the slide bed by integrating the seismic acceleration of the Longtoushan seismic station (Fig. 1a, about 9 km from the landslide site, and 3 km from the epicenter) recorded for the 2014 Ludian earthquake (Fig. 8).

# 4 Landslide Process and Mechanism

## 4.1 Fracture Evolution of the Landslide

The catastrophic process of landslides is induced by the accumulated internal damage and rupture growth. To study the evolution of fractures of the slide body during an earthquake, the fracture characteristics of the cohesive bonds between the particles in the slide body at different times are statistically analyzed. Figure 9 illustrates the evolution of the fracture ratio (FR) within 0.01 s interval and the total fracture ratio of the landslide with time. It can be seen from Fig. 9, prior to 3.0 s, the slope is in a stable state with no internal ruptures occurring subject to the weak seismic waves. With the gradual increase of seismic acceleration, the fracture ratio of a landslide develops sharply, especially the most sharply ones at 4.5–6 s. After that, it drops rapidly. In general, the landslide fracture ratio during 6–10 s is relatively low, while there is a sharp increase of the landslide fracture ratio at about 7 s, indicating that the landslide experiences a rapid failure within this period again. During 10–15 s, the landslide fracture ratio increases, indicating that the rock fracturing has intensified. After 15 s, the landslide fracture ratio drops gradually, and only a small number of fractures occur after 80 s. The ultimate fracture ratio of the landslide is about 2.75 $m^{-1}$.
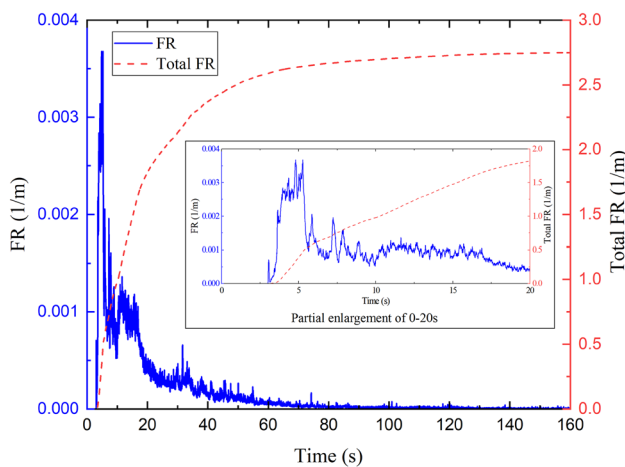
Figure 10 demonstrates the failure characteristics of the slide body at different times. The lower part of the landslide, which is composed of lower strength rocks, gradually fails first under the overburden pressure and intensified seismic loading (Fig. 10a). At about 5 s, fracturing occurs rapidly in this domain (Fig. 10b), resulting in a sharp increase of the landslide fracture ratio. Subsequently, the fractured rock starts to slide downward under gravity (Fig. 10c). Under seismic loading, the upper rock strata with higher strength also begin to break gradually (Fig. 10a, b). With the earthquake intensity increasing gradually, the fractures gradually develop and expand, which corresponds to a sharp increase of the landslide fracture ratio at about 8 s, which indicates that the upper rock strata are rapidly disintegrating and breaking (Fig. 10c). During the period of 8–10 s, the overall fracture characteristics of the upper rock strata do not change significantly. However, they are accompanied by the development of local fractures, which also correspond to the relatively low fracture ratio of the landslide in this stage (Fig. 9). It also shows that the rupture of the upper rock strata of the landslide is completed at about 8 s. After the lower rock strata completely disintegrate, they slide down, leading to the upper rock strata losinge their support and gradually moving down under the action of gravity and seismic activity. In the process of sliding, the upper rock strata fracture and disintegrate (Fig. 10d–h); specifically, at about 10–15 s, the upper rock strata disintegrate further due to the impact of the slide as these move downward (Fig. 10d, e). This is represented as an upward trend in the landslide fracture (Fig. 9). After 15 s, slipping dominates, accumulating and blocking the river, whereby the active disintegration of the landslide is completed. In this process, the fracture ratio decreases gradually. At about 160 s (Fig. 11), landslide accumulation and river blocking are completed, forming a landslide dam. In summary, it can be seen that, similar to the rock failure, the failure and disintegration of the landslide under seismic activity are due to the accumulation of internal damage in the rock strata that develops rapidly.

The geological structure of a landslide dam is one of the most important features to understand the stability or failure of it. Figure 11 presents the damage and fracture characteristics of the rock strata of the landslide dam. As shown, there are still some large-scale rock blocks, remaining on the upper part of the dam, while all of the rock blocks at the lower part have disintegrated. The fracture characteristics of the rock strata based on the numerical results are similar to that of the field investigation of the dam (Fig. 1c). Therefore, the numerical results presented in this study can be used to describe the engineering geological structure of the landslide dam and rapidly assess the geological structures of the landslide dam blocking the river.
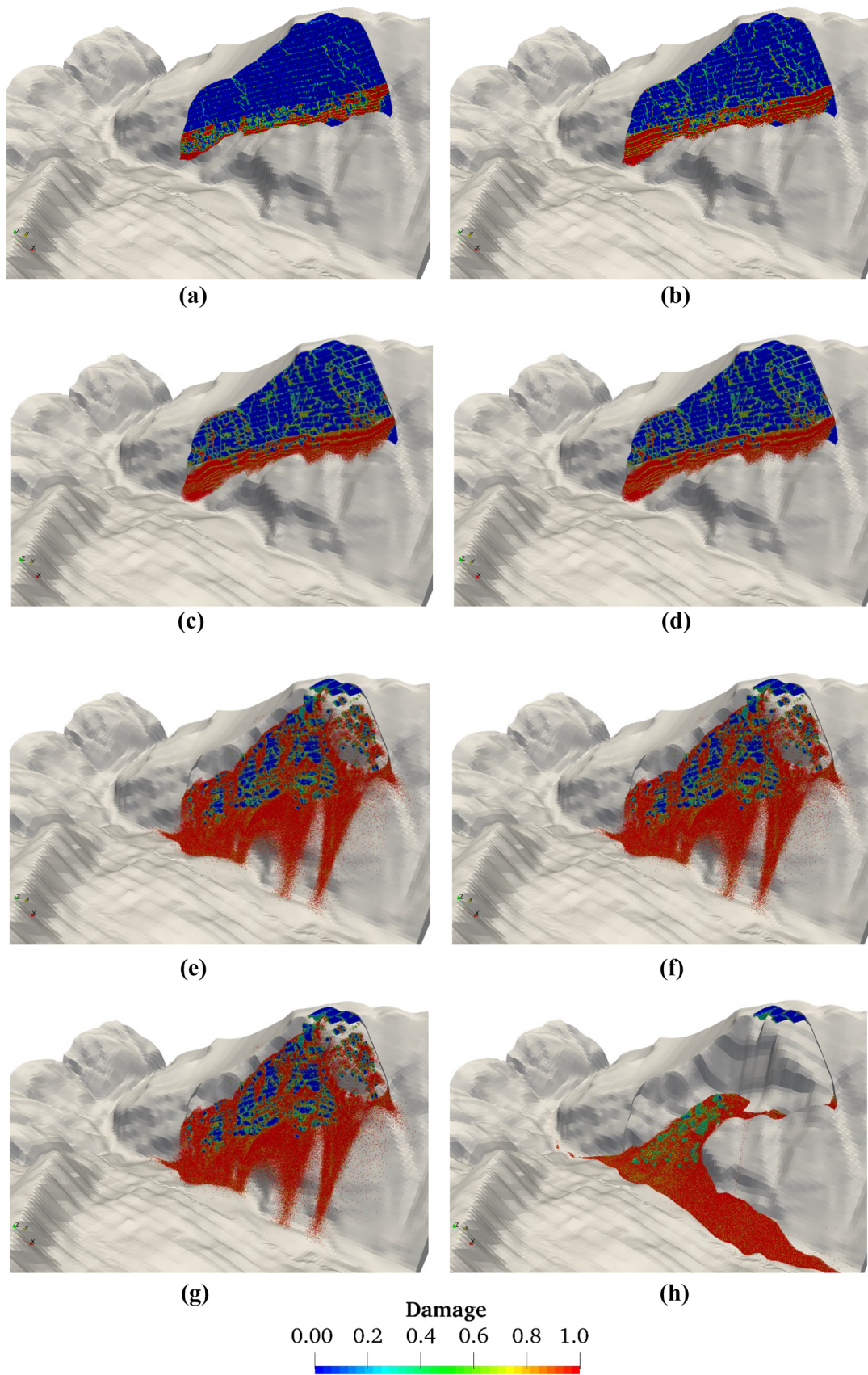


**Fig. 9** Evolution of the failure ratio of the landslide body with time

**Fig. 10** Damage and fracture characteristics of the landslide body at different times: **a** 5 s; **b** 6 s; **c** 8 s; **d** 10 s; **e** 15 s; **f** 20 s; **g** 60 s; **h** 100 s
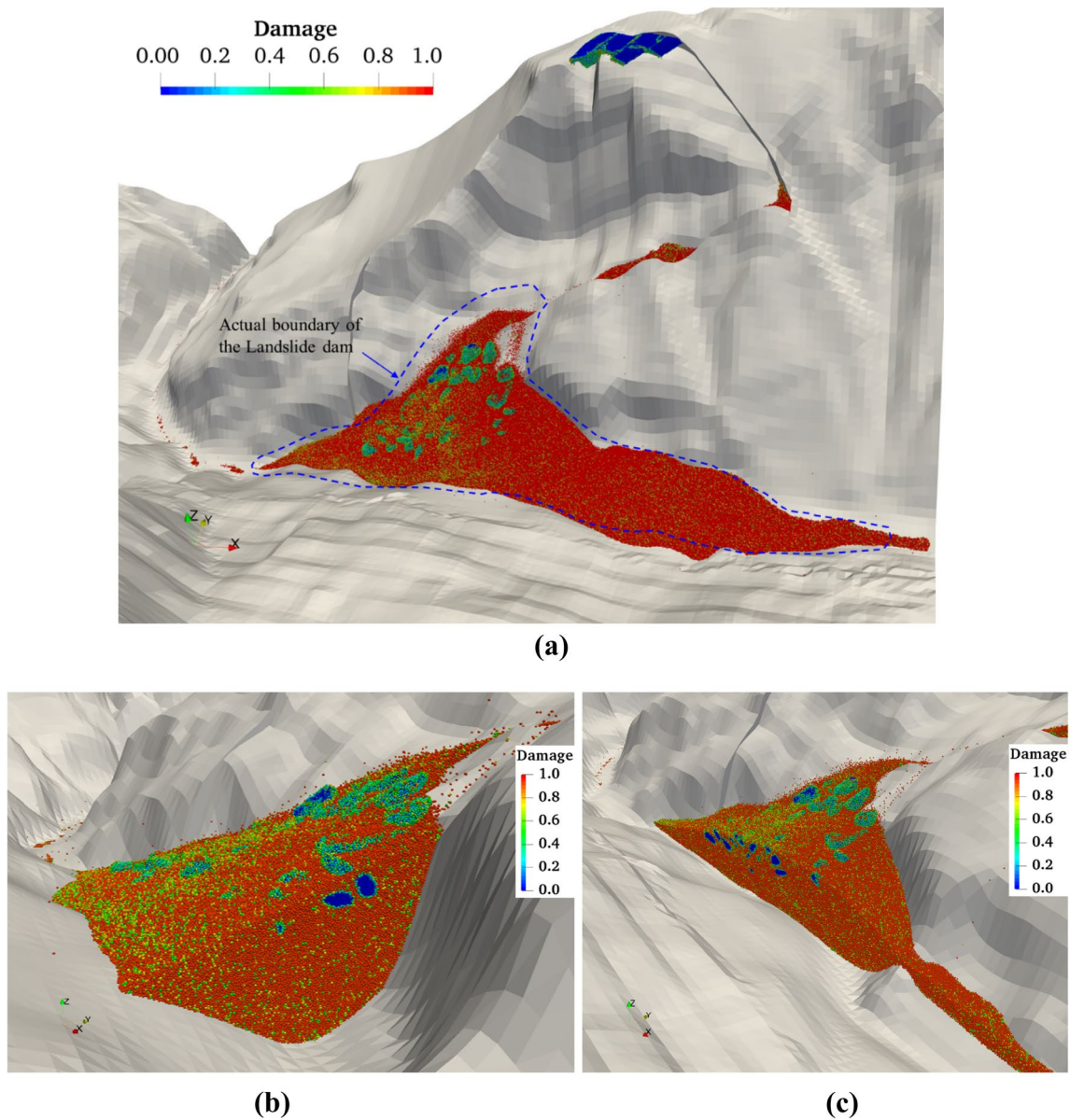
**Fig. 11** Damage and fracture characteristics of the rock strata at 160 s (damage = 0 implies original rock strata, while damage = 1 indicates disintegrated rock strata): **a** final shape of the landslide body; **b** cross section of the landslide body flowing across the river; **c** cross section of the landslide body flowing along the river

## 4.2 Kinematics of the Landslide

Landslide kinematics is one of the most important subjects to study the disaster. To study the kinematic behaviors of the Hongshiyan landslide during the failure process under the earthquake, four monitoring sections were identified in the slide body to monitor the movement of 20 blocks (Fig. 12).

Figure 13 shows the velocity evolution of each monitoring block with time, and Fig. 14 shows the velocity distribution of the landslide at different times in DEM simulation. It can be seen from Fig. 13 that the motions of blocks No.1, 2, 7–10 and 16–20 are similar: they all reach a peak value

rapidly in different periods (at the speed of over 40 m/s) and then drop sharply to 0 m/s. The blocks located at the front edge of the landslide body reach the maximum value first. For the influence of the slope morphology and the lower soft rock (Fig. 5b), the soft rock strata near the monitoring block No. 20 slide firstly at a high speed (Fig. 14b) and rapidly reach the bottom, impacting the riverbed, and the speed decreases sharply to zero in the process. The rest of the monitoring blocks located in the middle and rear of the landslide body do not show significant velocity variation, although the velocities of different points are different before 10 s, especially as the upper rock strata tend to move

**Fig. 12** Spatial distribution of the monitoring blocks
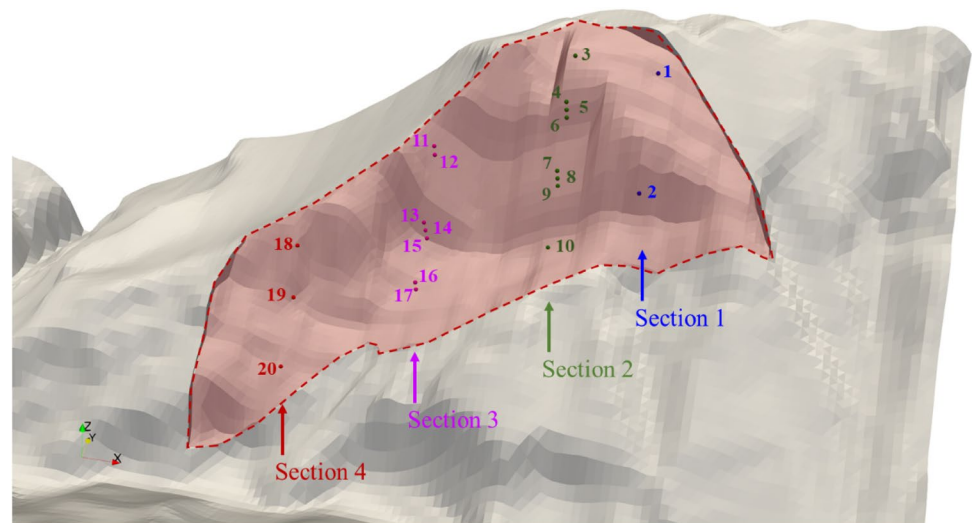


synchronously (Figs. 13, 14a–c). The results indicate that at the initial stage under the influence of the earthquake, the landslide body moves as a whole with the velocity increasing gradually. After the disintegration of the landslide body, each part begins to differentiate in motion and the velocity increases rapidly under gravity. As a result of the steep free surface in front of the landslide body, the rock strata located at the front accelerate freely under gravity and first reach the bottom. After impacting the riverbed, the landslide rocks accumulate on the riverbed. In particular, the rock strata at the front edge of monitoring sections 1, 2 and 3 have high potential energy and steep free surface of slope, which result in large kinetic energy with high velocities before impact. The rock strata located at the middle and rear part of the landslide body tends to move as a whole before 15 s (Figs. 13b, c, 14a–c); and the movements of the rock begins to show obvious differentiation due to the gradual fracture and disintegration of the rock strata. In the running process, it is affected by the shape of the bottom sliding bed and the accumulation of the lower rock strata in the riverbed. The velocity reaches the maximum value (about 20 m/s) at about 15 s, and then drops gradually. The rock strata at the rear of the landslide body show a trend of accelerated motion under gravity after 60 s, which is mainly due to this part of the rock strata reaching the steep free surface of the slope at the front edge of the landslide body at about 60 s.

An in-depth study of the landslide movements at different times (Fig. 15) reveals that the velocity of each block within the monitoring section 2 varies with time. It can be seen that before 8 s, except for the lower soft rock strata of monitoring block No. 10, the remaining monitoring blocks move at the same speed; after 10 s, the velocity of the monitoring blocks (No. 4–10) in the upper rock strata begins to vary. For the rock strata at the same section with different elevations, before reaching the peak velocity, the lower part

moves faster than the upper part, particularly for the velocity along the slope (Fig. 15b) and vertically (Fig. 15c). At different locations, the rock strata at the front edge move at a higher speed. From Fig. 15c, it can be seen that at about 15 s, the vertical movement of middle blocks (No. 7, 8 and 9) slows down rapidly, which is mainly due to the part of the rock strata at the landslide front (Fig. 14c, d) that is blocked by a flattened sliding surface (Fig. 12). After that, the rock strata run out of the slide face, slide down along the lower steep slope free surface, accelerate again under gravity and eventually accumulate on the riverbed. The rock strata (No. 4, 5 and 6) at the rear slide along the slide face before 60 s, influencing the sliding of rock strata at the front landslide body. During this process, they reach a peak velocity at about 15 s and then slow down gradually. At about 60 s, this part of the rock strata rushes out of the slide face and moves along the free surface at the lower steep slope. It accelerates under the gravity and eventually accumulates in the valley after impacting the riverbed. Overall, the upper rock strata tend to move downstream along the river (in the negative direction of $x$) as a result of the influence by the occurrence of rock strata and the spatial form of the slide face (Fig. 15a). Therefore, the maximum thickness of the landslide dam is located at downstream along the river rather than at the location of the central section of the landslide body (Fig. 16).

### 4.3 Mechanism of Landslide

The Hongshiyan landslide is a kind of typical anti-dip rock slope with a low dip angle. Generally, this kind of slope is stable. However, under these circumstances a typical weak base geological structure is formed, because the lower part of the landslide body is supported by a soft stratum that contains shale inter-bedded with sandstone. Furthermore, with the influence of unloading and weathering, two sets of

**Fig. 13** Velocity evolutions of the monitoring blocks along different cross sections: **a** sections 1 and 4; **b** section 2; **c** section 3
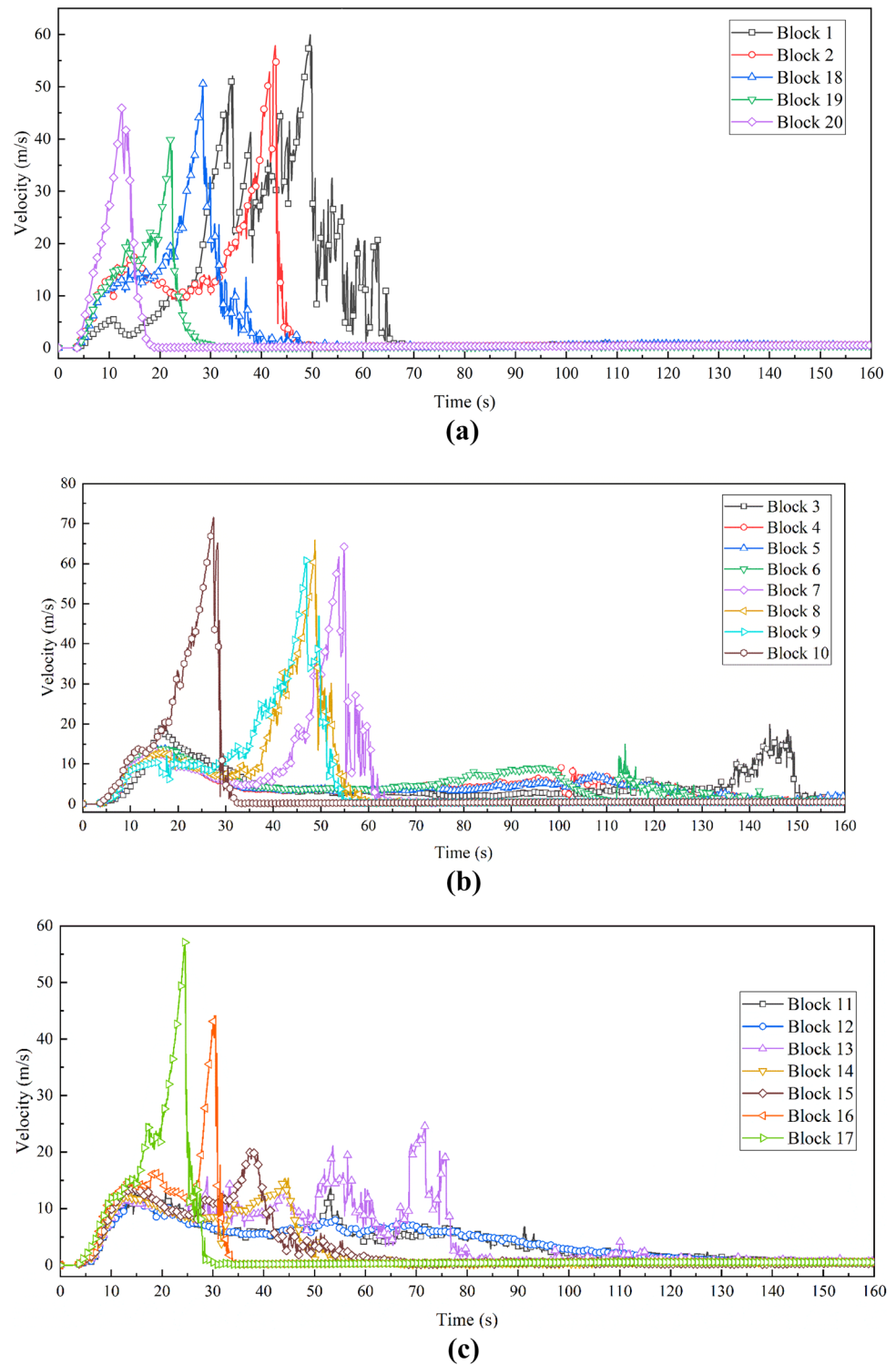


steep-dipping fractures develop in the shallow part of the slope, which constitutes the internal factors of the landslide.

Induced by an intense earthquake, on one hand, there is variation in the movement of layered rock at different spatial positions due to the topography and rock structure. Consequently, internal damages of the rock strata accumulate continuously and seismic fractures are produced (Fig. 15a). On the other hand, the weak rock strata in the lower part of the landslide are firstly broken under the pressure of the upper rock strata during the earthquake, and then flow out (Fig. 15a–c), which results in the supporting loss of the upper rock strata and increases the differential interlayer
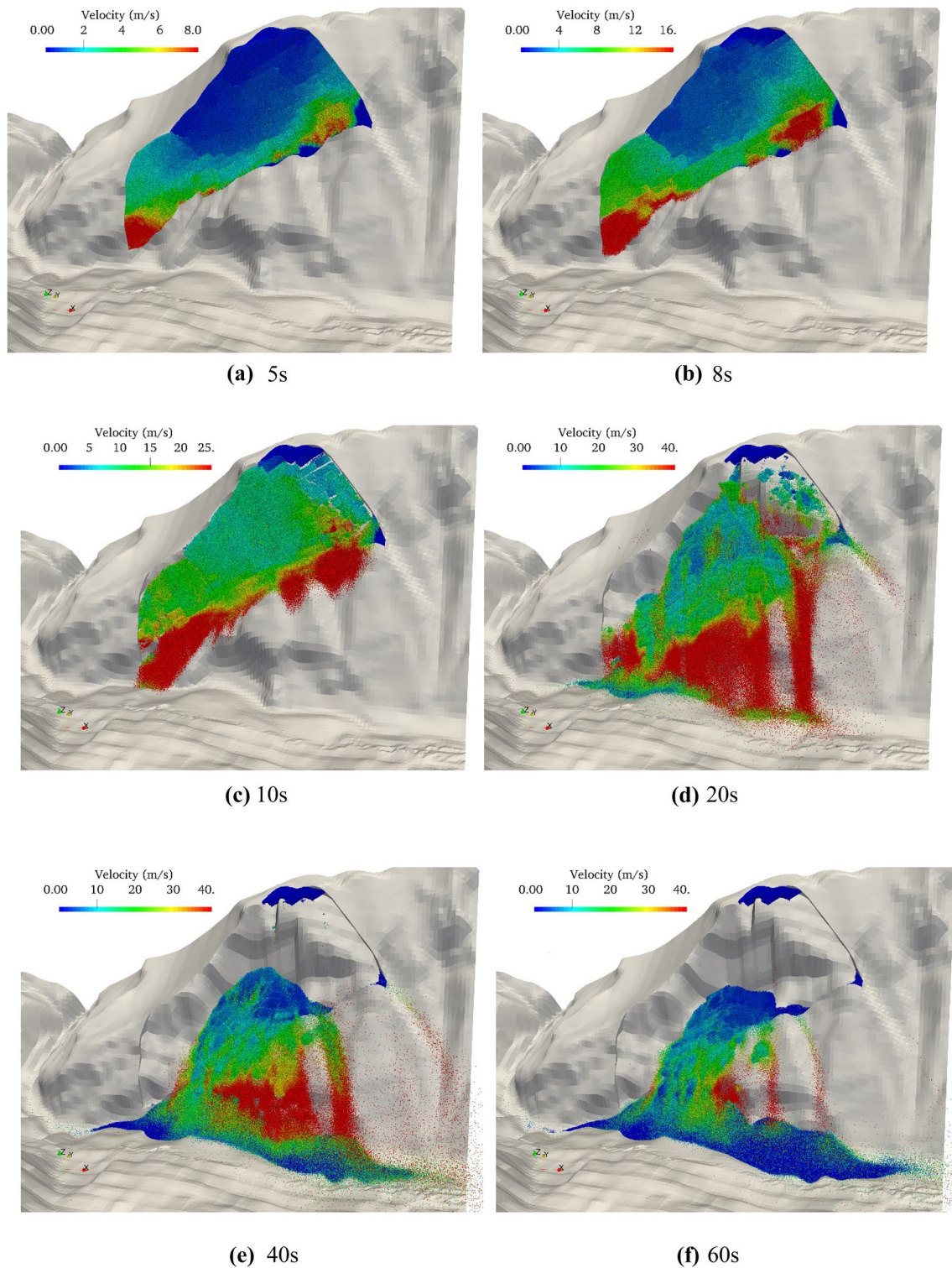
**(a)** 5s

**(b)** 8s

**(c)** 10s

**(d)** 20s

**(e)** 40s

**(f)** 60s

**Fig. 14** Velocity of the landslide at different times: **a** 5 s; **b** 8 s; **c** 10 s; **d** 20 s; **e** 40 s; **f** 60 s

movement of the upper rock strata (Fig. 15c). With the lower soft rocks sliding out continuously, the upper rock strata start to slide downward at a high speed, following by dislocation, impact and fragmentation (Fig. 15d–f). In

the process of falling and accumulating of the upper rock strata, the materials accumulated in the riverbed elevate the base and reduce the potential energy relative to accumulated rock. Meanwhile, the rock strata accumulated at the lower
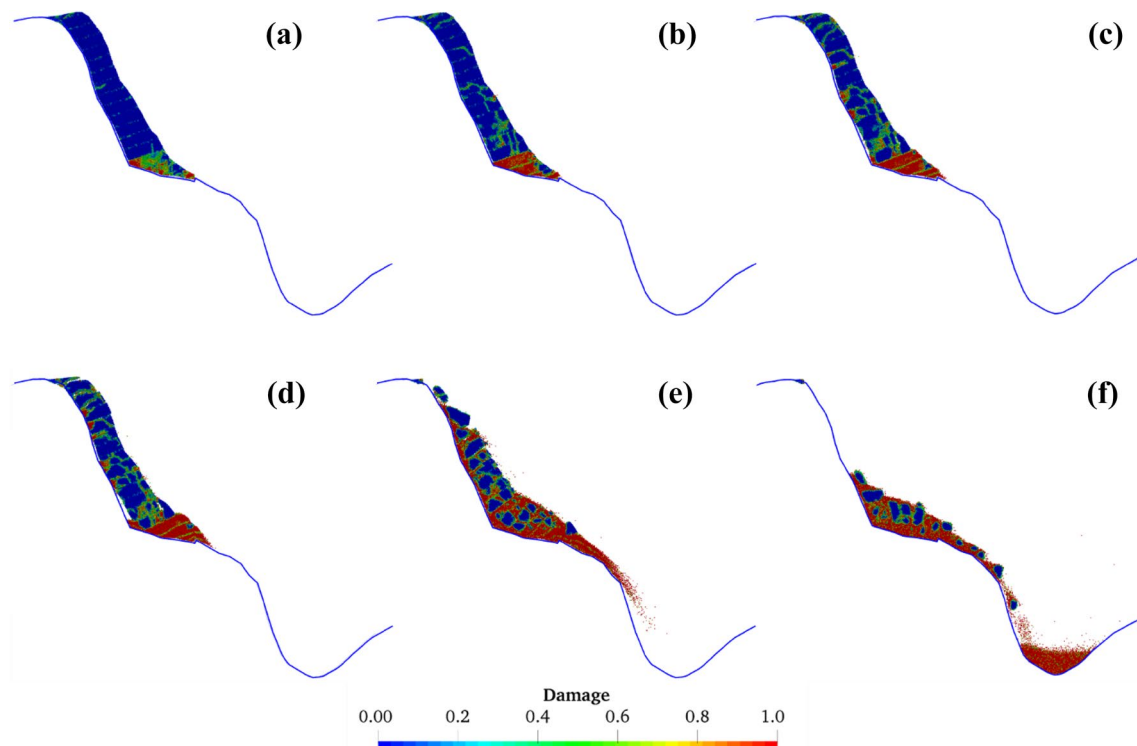
(a)



(b)



(c)
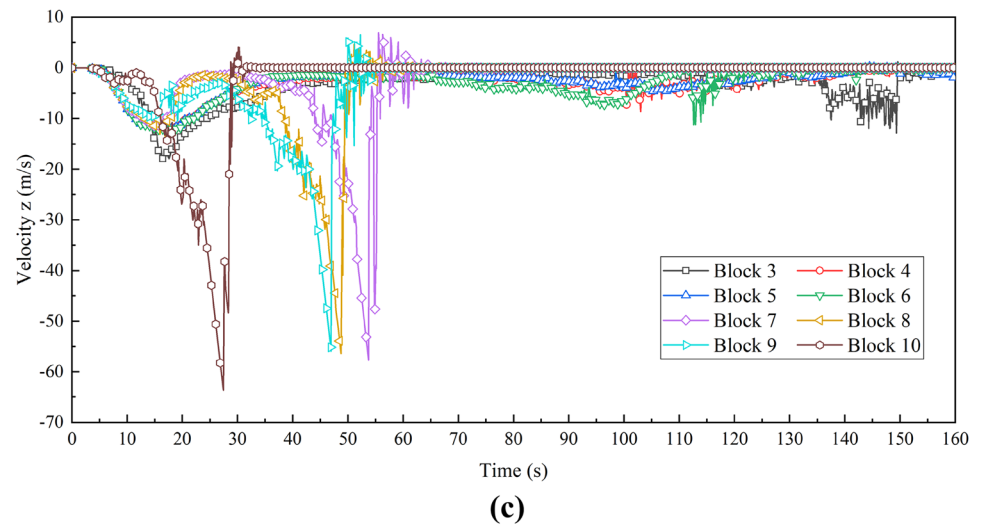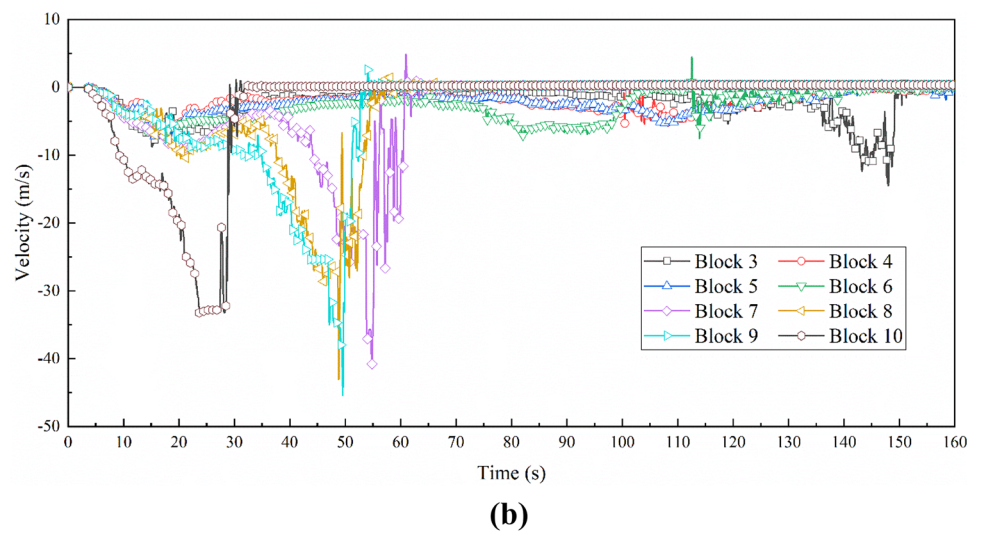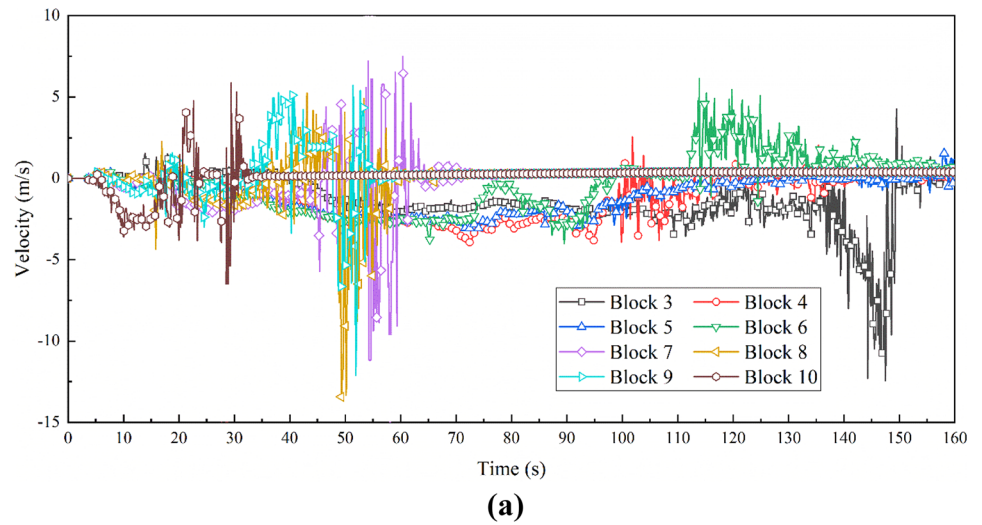
**Fig. 16** The failure model of the slope under earthquake: **a** 5 s; **b** 6 s; **c** 8 s; **d** 10 s; **e** 20 s; **f** 40 s

elevation buffer the newly accumulated rock strata. Due to the high strength of the upper rock strata, the rock breakage of the upper part of the landslide dam is low, resulting in the geological structure characteristics of the landslide dam presents "fine particles at the lower elevation and coarse rock blocks at the higher elevations", which is in agreement with the field investigation.

The geological structure of the slope soft base is an important internal factor in the process of the collapse, disintegration and slide at a high speed, while the intense earthquake is the controlling external factor that induces the rock strata to break and disintegrate. With the effects of the earthquake, as the rock strata begin to slide downward, the high-speed movement and accumulation process of the landslide is not controlled by the earthquake, but is mainly controlled by the geological structure of the landslide body and the topography of the valley (Fig. 15d–f). The anti-dip rock does not slide downward along the bedding plane, but breaks continuously during sliding (Fig. 15), which is different from the failure mode of the bedding rock landslide.

## 5 Discussion and Reflection

In this study, the failure process of the 2014 Hongshiyan landslide is reproduced by using 3D DEM, and the kinematics and mechanisms of the landslide are systematically

studied, which can be challenging just based on the field investigations. Based on the results of this study, there are some meaningful contents that need to be disseminated.

### 5.1 Numerical Method

For the advantages in the simulation of discontinuous body, DEM has been widely used in the study of landslide kinematics. In DEM, the simulated domain should be divided into an assembly of particles. Spherical particles are common and computationally efficient to resolve inter-particle contact. In this study, a 3D DEM model generation method of landslides based on spherical particles is proposed. It is known that by using the spherical particle DEM, the particle size, shape and the compactness of the assembly may have an effect on the numerical results (Donze et al. 2009).

For the compactness, a pre-compression method with smooth particles is used during the model generation. The contact stiffness of the particles influences the compaction, and therefore it should be estimated from laboratory tests. Generally, the contact stiffness between DEM particles of the rock material is higher than that of the soil, to obtain a tightly contacted particles' assembly a higher initial compression stress should be used. In this study, a pre-compression stress of 1 MPa is used (generally, 200 kPa is used for soil material). However, the pre-compression stress should not be too large, because in DEM, for particles with the same

contact stiffness, the higher the pre-compression stress, the larger is the penetration distance, and higher will the contact forces exist between the particles. As the outer boundary of the landslide body (Fig. 4) is removed after the model generation, relaxation of the confining boundary results in the contact forces to act as the repulsive forces between particles. Hence, if the contact forces are larger than the contact strength of the particles, the bond between the contacted particles will break, and the model assembly may collapse.

In DEM, the size of the spherical particles may also influence the numerical results, especially if the particle's size is larger relative to the scale of the simulated domain. However, it is computationally intractable to simulate a landslide with the same size of the "real" particles when using DEM. Hence, these two factors should be considered at the same time. First and most importantly, the particle size should be far less than the characteristic scale ($L_c$) of the simulated domain. The $L_c$ of a landslide is its thickness; and the $L_c$ of a sample for the triaxial test is its diameter. According to the previous studies (Ding et al. 2014), when the ratio of the maximum size of the particle to the $L_c$ is larger than 1/20, there are few influences of the particles' size on the numerical results. In this study, the maximum size of the spherical particles is about 1/27 times of the landslide's $L_c$ (about 60 m). The second is the calculation cost that is dependent on the code used for the simulation. In this study, about 295,985 spherical particles are used. This takes about 1 week of computation to model 160 s of simulation using YADE on a workstation with 8 CPUs.

It is impractical to obtain the contact parameters of DEM particles by experiments directly. Generally, the DEM particles' size is much larger than the "real" particles. In this study, an inversion method is introduced. Firstly, laboratory tests of rock samples obtained from the landslide area were performed. Since the limitation of the laboratory test, the size of the sample is only 5 cm in diameter and 10 cm in height. The DEM particle's size is much larger than the size of the rock sample of the laboratory test. It is known that if the inhomogeneity's and cracks of the rock sample are not considered, there is very little influence of the sample scale on its stress–strain relationship. Hence, a sample of a diameter of 40 m and 80 m in height is used for the DEM numerical test of the particle's parameters inversion. However, for the action of the geological processes, a lot of discontinuities exits in a landslide body and other geologic bodies, which will make the actual mechanical parameters different from that of the laboratory test. These discontinuities also are the main difficulties for all the numerical methods. It is suggested that new methods should be developed, for example, using machine learning to revise the parameters inversed based on laboratory tests according to the results of the field monitoring and investigation of the deformation and failure characteristics.

## 5.2 Geological Structure of the Landslide Dam

For the river blocking disaster of a landslide, analysis of the stability and breach process of the landslide dam is very important to rapidly determine the geological structure of the formed landslide. The geological structure of the landslide dam is mostly controlled by the geological structure of the slide body, sliding distance and topography of the valley. For the higher speed and short run-out distance of the landslide, the geological structure of the slope may greatly control the structure of the landslide dam. For the slope of bedding rock, the bedding plane will control the failure process, and the formed landslide dam is characterized as "coarse rock blocks at the lower elevations and fine particles at the higher elevations" of the landslide dam (Xu et al. 2013). While for the slope of anti-dip rock the bedding plane will not control the movement of the landslide, the geological structure of the landslide dam is characterized by the formation of the fine particles at the lower elevations of the landslide dam, while coarse rock blocks are mainly limited to the higher elevations of the landslide dam.

## 6 Conclusions

River blocking is a common secondary disaster in a disaster chain following the onset of a landslide due to seismic loading. The geological structure of the landslide dam determines its stability and dam breaching process. Intense earthquakes are a critical external factor for inducing landslides. In this study, the Hongshiyan landslide is considered by study of the onset, movement, river blocking and formation of the landslide dam under intense seismic activity. The results obtained are significant to understand landslide disaster dynamics in valley areas. Field investigations on the Hongshiyan landslide revealed a typical weak base anti-dip rock slope, in which the data are available to construct a 3D DEM model of the geological structure of the slope.

Inversion tests were conducted to obtain the DEM model parameters by means of data obtained from the triaxial experiments which are performed on rocks that are recovered from the landslide. The failure of the Hongshiyan landslide under seismic activity is then reproduced using the 3D DEM simulation. The seismic damage, landslide body fracturing and landslide dynamics are systematically studied. The fracture and disintegration of the slide body under seismic loading is the result of the damage accumulation of rock strata, which develops rapidly, that is, the rupture and disintegration is essentially instantaneous. The soft rock at the lower part of the slope breaks first under seismic loading and then flows under pressure of the upper rock strata. This leads to further failure and disintegration of the upper layered rock

strata of the slope. The weak base is an important internal factor for the failure of the Hongshiyan landslide. In addition, the anti-dip rock structure makes the slide failure mode and kinematic behavior distinct from rock bedding of the landslide that results in the formation with "fine particles at the lower part of the dam, while coarse rock blocks at primarily confined to the elevated part of the dam". Based on the numerical simulation presented in this study, the process and understanding of this is revealed.

The landslide triggering and failure mode mostly depends on the external factors, while the subsequent dynamic process of the landslide and the engineering geological structure of the landslide dam depend mainly on the geological structure of the slide body, sliding distance and topography of the valley.

**Author Contributions** WJX performed the numerical simulations of this study and wrote the manuscript. LW performed the laboratory test of the rock sample used in this study. KC performed the geological analysis and field investigation of the landslide.

# References

Barla M, Piovano G, Grasselli G (2012) Rock slide simulation with the combined finite-discrete element method. Int J Geomech 12(6):711–721

Bozzano F, Lenti L, Martino S et al (2011) Earthquake triggering of landslides in highly jointed rock masses: reconsruction of the 1783 Scilla rock avalanche (Italy). Geomrphology 129:294–308

Chang ZF, Chen XL, An XW et al (2016) Contributing factors to the failure of an unusually large landslide triggered by the 2014 Ludian, Yunnan, China, Ms = 6.5 earthquake. Nat Hazards Earth Syst Sci 16(497–507):2016

Cundall PA, Strack OD (1979) A discrete numerical model for granular assemblies. Géotechnique 29(1):47–65

Dai ZL, Huang Y, Cheng HL, Xu Q (2011) 3D numerical modeling using smoothed particle hydrodynamics of flow-like landslide propagation triggered by the 2008 Wenchuan earthquake. Eng Geol 4(180):21–33

Ding XB, Zhang LY, Zhu HH et al (2014) Effect of model scale and particle size distribution on PFC3D simulation results. Rock Mech Rock Eng 47(6):2139–2156

Donze FV, Richefeu V, Magnier SA (2009) Advances in discrete element method applied to soil rock and concrete mechanics. Electron J Geotech Eng 8:1–44

Fan XM, Juang CH, Wasowski J et al (2018) What we have learned from the 2008 Wenchuan Earthquake and its aftermath: a decade of research and challenges. Eng Geol 241:25–32

Feng ZY, Lo CM, Lin QF (2017) The characteristics of the seismic signals induced by landslides using a coupling of discrete element and finite difference methods. Landslides 14:661–674

Harp EL, Jibson RW (1996) Landslides triggered by the 1994 Northridge, California, earthquake. Bull Seismol Soc Am 86(1B):S319–S332

Ivars DM, Potyondy DO, Pierce M, Cundall PA (2008) The smooth-joint contact model. In: Proceeding of the 8th world congress on computational mechanics and 5th European congress on computational methods in applied sciences and engineering at: Venice, Italy, p 2735

Luo J, Pei XJ, Evans SG et al (2019) Mechanics of the earthquake-induced Hongshiyan landslide in the 2014 Mw 6.2 Ludian earthquake, Yunnan, China. Eng Geol 251:197–213

Keefer DK (2002) Investigating landslides caused by earthquakes—a historical review. Surv Geophys 23(6):473–510

Kozicky J, Donze FV (2009) YADE-OPEN DEM: an open-source software using a discrete element method to simulate granular material. Eng Comput 26(7):786–805

Lin CH, Lin ML (2015) Evolution of the large landslide induced by Typhoon Morakot: a case study in the Butangbunasi River, southern Taiwan using the discrete element method. Eng Geol 197:172–187

Lo CM, Lin ML, Tang CL et al (2011) A kinematic model of the Hsiaolin landslide calibrated to the morphology of the landslide deposit. Eng Geol 123(1–2):22–39

Scholtes L, Donze FV (2012) Modelling progressive failure in fractured rock masses using a 3D discrete element method. Int J Rock Mech Min Sci 52:18–30

Scholtes L, Donze FV (2015) A DEM analysis of step-path failure in jointed rock slopes. CR Mec 343:155–165

Smilauer V et al (2015) Yade documentation, 2nd ed. The Yade Project. 10.5281/zenodo.34073 (http://yade-dem.org/doc/)

Song YX, Huang D, Cen DF (2016) Numerical modelling of the 2008 Wenchuan earthquake-triggerd Daguangbao landslide using a velocity and displacement dependent friction law. Eng Geol 215:50–68

Tang CL, Hu JC, Lin ML et al (2009) The Tsaoling landslide triggered by the Chi-Chi earthquake, Taiwan: insights from a discrete element simulation. Eng Geol 106(1–2):1–19

Wang HL, Liu SQ, Xu WY et al (2020) Numerical investigation on the sliding process and deposit feature of an earthquake-induced landslide: a case study. Landslides 17:2671–2682

Wu JH (2010) Seismic landslide simulations in discontinuous deformation analysis. Comput Geotech 37(5):594–601

Wu JH, Do TN, Chen CH et al (2017) New geometric regulation for the displacement constraint points in discontinuous deformation analysis. Int J Geomech 17(5):E4016002

Wu JH, Lin WK, Hu HT (2018) Post-failure simulations of a large slope failure using 3DEC: the Hsien-du-shan slope. Eng Geol 242:92–107

Xu WJ, Xu Q, Wang YJ (2013) The mechanism of high-speed motion and damming of the Tangjiashan landslide. Eng Geol 157:8–20

Xu XW, Xu C, Yu GH et al (2015) Primary surface ruptures of the Ludian Mw 6.2 earthquake, southeastern Tibetan Plateau, China. Seismol Res Lett 86(6):1622–1635

Yamagishi H, Yamazaki F (2018) Landslides by the 2018 Hokkaido Iburi-Tobu Earthquake on September 6. Landslides 15(12):2521–2524

Zhang YB, Chen GQ, Zheng L et al (2013) Effects of near fault seismic loadings on run-out of large-scale landslide: a case study. Eng Geol 166:216–236

Zhou YY, Shi ZM, Zhang QZ et al (2019) 3D DEM investigation on the morphology and structure of landslide dams formed by dry granular flows. Eng Geol 258:105151